Supporting Information

Predicting the Second-Order Nonlinear Optical Responses of Organic Materials: the Role of Dynamics

Frédéric Castet[1*], Claire Tonnelé[2*], Luca Muccioli[3*], Benoît Champagne[4*]

[1] Univ. Bordeaux, CNRS, Bordeaux INP, ISM, UMR 5255, F-33400 Talence, France. [2] Donostia International Physics Center (DIPC), Manuel Lardizabal Ibilbidea 4, 20018 Donostia, Euskadi, Spain. [3] Department of Industrial Chemistry ''Toso Montanari'', University of Bologna, Viale Risorgimento 4, 40136 Bologna, Italy. [4] Unité de Chimie Physique Théorique et Structurale, Chemistry Department, Namur Institute of Structured Matter, University of Namur, , Rue de Bruxelles 61, 5000 Namur, Belgium.

Emails: frederic.castet@u-bordeaux.fr, claire.tonnele@dipc.org, luca.muccioli@unibo.it, benoit.champagne@unamur.be

Expressions for $\langle\beta_{ZZZ}^2\rangle$, $\langle\beta_{ZXX}^2\rangle$, $\gamma_{//}$, and $\beta_{//}$ in the molecular frame

In the following equations, the molecular frame cartesian axes are labelled η, χ and ξ while the laboratory frames axes X, Y, Z.

The components of the hyperpolarizability tensor relevant for the HRS response are:

$$\langle\beta_{ZZZ}^2\rangle = \frac{1}{7}\sum_{\zeta}^{x,y,z}\beta_{\zeta\zeta\zeta}^2 + \frac{4}{35}\sum_{\zeta\neq\eta}^{x,y,z}\beta_{\zeta\zeta\eta}^2 + \frac{2}{35}\sum_{\zeta\neq\eta}^{x,y,z}\beta_{\zeta\zeta\zeta}\beta_{\zeta\eta\eta} + \frac{4}{35}\sum_{\zeta\neq\eta}^{x,y,z}\beta_{\eta\zeta\zeta}\beta_{\zeta\zeta\eta} + \frac{4}{35}\sum_{\zeta\neq\eta}^{x,y,z}\beta_{\zeta\zeta\zeta}\beta_{\eta\eta\zeta} + \frac{1}{35}\sum_{\zeta\neq\eta}^{x,y,z}\beta_{\eta\zeta\zeta}^2 + \frac{4}{105}\sum_{\zeta\neq\eta\neq\xi}^{x,y,z}\beta_{\zeta\zeta\eta}\beta_{\eta\xi\xi} + \frac{1}{105}\sum_{\zeta\neq\eta\neq\xi}^{x,y,z}\beta_{\eta\zeta\zeta}\beta_{\eta\xi\xi} + \frac{4}{105}\sum_{\zeta\neq\eta\neq\xi}^{x,y,z}\beta_{\zeta\zeta\eta}\beta_{\xi\xi\eta} + \frac{2}{105}\sum_{\zeta\neq\eta\neq\xi}^{x,y,z}\beta_{\zeta\eta\xi}^2 + \frac{4}{105}\sum_{\zeta\neq\eta\neq\xi}^{x,y,z}\beta_{\zeta\eta\xi}\beta_{\eta\zeta\xi} \quad \text{(S1)}$$

and

$$\langle\beta_{ZXX}^2\rangle = \frac{1}{35}\sum_{\zeta}^{x,y,z}\beta_{\zeta\zeta\zeta}^2 + \frac{8}{105}\sum_{\zeta\neq\eta}^{x,y,z}\beta_{\zeta\zeta\eta}^2 + \frac{4}{105}\sum_{\zeta\neq\eta}^{x,y,z}\beta_{\zeta\zeta\zeta}\beta_{\zeta\eta\eta} - \frac{2}{35}\sum_{\zeta\neq\eta}^{x,y,z}\beta_{\eta\zeta\zeta}\beta_{\zeta\zeta\eta} - \frac{2}{35}\sum_{\zeta\neq\eta}^{x,y,z}\beta_{\zeta\zeta\zeta}\beta_{\eta\eta\zeta} + \frac{3}{35}\sum_{\zeta\neq\eta}^{x,y,z}\beta_{\eta\zeta\zeta}^2 - \frac{2}{105}\sum_{\zeta\neq\eta\neq\xi}^{x,y,z}\beta_{\zeta\zeta\eta}\beta_{\eta\xi\xi} + \frac{1}{35}\sum_{\zeta\neq\eta\neq\xi}^{x,y,z}\beta_{\eta\zeta\zeta}\beta_{\eta\xi\xi} - \frac{2}{105}\sum_{\zeta\neq\eta\neq\xi}^{x,y,z}\beta_{\zeta\zeta\eta}\beta_{\xi\xi\eta} + \frac{2}{35}\sum_{\zeta\neq\eta\neq\xi}^{x,y,z}\beta_{\zeta\eta\xi}^2 - \frac{2}{105}\sum_{\zeta\neq\eta\neq\xi}^{x,y,z}\beta_{\zeta\eta\xi}\beta_{\eta\zeta\xi} \quad \text{(S2)}$$

In the EFISHG response, $\beta_{//}$ and $\gamma_{//}$ are also defined as combinations of molecular hyperpolarizability tensor elements. $\beta_{//}$ is related to the projection of the vectorial representation of the β tensor, $\boldsymbol{\beta}$, on the permanent dipole moment vector $\boldsymbol{\mu}_0$:

$$\beta_{//}(-2\omega;\omega,\omega) = \beta_{//} = \frac{3}{5}\frac{\boldsymbol{\mu}_0\cdot\boldsymbol{\beta}}{\mu_0} = \frac{3}{5}\sum_{\zeta}\frac{\mu_{0\zeta}\beta_{\zeta}}{\mu_0} \quad \text{(S3)}$$

where the hyperpolarizability vector components are defined as:

$$\beta_{\zeta} = \frac{1}{3}\sum_{\eta}(\beta_{\zeta\eta\eta} + 2\beta_{\eta\zeta\eta}) \quad \text{(S4)}$$

Analogously, $\gamma_{//}$ corresponds to the isotropic invariant of the γ tensor:

$$\gamma_{//}(-2\omega;\omega,\omega,0) = \gamma_{//} = \frac{1}{15}\sum_{\zeta\eta}(2\gamma_{\zeta\zeta\eta\eta} + \gamma_{\zeta\eta\eta\zeta}) \quad \text{(S5)}$$

Convergence of Molecular Dynamics simulation averages

Following a sequential MD+QM approach, one ends up with a discrete time series $A(t)$ of a physical property A (here typically a function of the hyperpolarizability tensor components) of N values sampled at regular time intervals of period Δt. Its time average is then $\langle A \rangle = \frac{1}{N}\sum_{i=1}^{N} A(i\Delta t)$, its mean square is $\langle A^2 \rangle = \frac{1}{N}\sum_{i=1}^{N}[A(i\Delta t)]^2$ and its variance $\sigma^2 = \langle A^2 \rangle - \langle A \rangle^2$.

Though, how to check whether $N \times \Delta t$ is long enough? Has equilibrium been reached and what is the error associated to averages?

The mathematical problem of assessing the convergence of discrete time series is an important branch of the signal processing discipline. Here we refer the interested reader to textbooks while limiting our discussion to simple methods to quickly verify that simulation results are not too far from convergence, or in other words, that our time series does not contain strong correlations.[1] This assessment is important for any simulation observable and particularly for quantities, like hyperpolarizabilities, that exhibit large fluctuations in time and space coordinates.

To provide a practical example, we selected as a test system one azobenzene molecule in gas phase, and its β_{HRS} as the physical property of interest. Azobenzene possesses an inversion center at its *trans* equilibrium geometry, hence its second-order NLO response should be strictly zero if dynamic effects are not considered. This is indeed the case at equilibrium geometries, as shown in Table S1 for DFT and two different force fields, where the small deviations from zero originate from numerical approximations (on the atomic Cartesian coordinates, and therefore on the symmetry). Adding the contribution of vibrational motions with MD simulations gives rise to a small but still sizable HRS signal, with standard deviations as large as the signal itself, which in turn are magnified in near resonance conditions with the second

harmonic wavelength when the dynamic response is calculated. Notice that, since occasional resonances give rise to some very large outliers, robust measures of scale such as the interquartile range are more adapted than standard deviation to characterize the shape of the distribution (Table S1, dynamic MD results). Always in Table S1, the considerably different results recorded with standard GAFF parameters and refined ones highlight the importance of the FF parameterization in the result.

Coming back to the convergence of dynamics values, the crudest test is the visual inspection of the trends of cumulative moving averages, e.g. $CMA(t = k\Delta t) = \frac{1}{k}\sum_{i=1}^{k\leq N} A(i\Delta t)$, which should reach a plateau at $\langle A \rangle$ at long times (for $k \to N$, see e.g. Figure S1, blue line). This is an indication that the data set is large enough, i. e. that increasing N will not change the value of the global average $\langle A \rangle$. Obviously, longer times are required for the convergence of $\langle A^2 \rangle$ and σ^2.

A more quantitative approach consists in computing block averages on M_B blocks of data of increasing size $B = 1, 2, \ldots, N$. Each block j of size B has average $A_{j,B}$, and for each size, the variance of the block averages is evaluated as $\sigma_B^2 = \frac{1}{M_B}\sum_{j=1}^{M_B}\left(A_{j,B} - \langle A \rangle\right)^2$. It turns out that for large block sizes, $\sigma_B/\sqrt{M_B}$ is a good estimator of the standard deviation of the mean $\sigma_{\langle A \rangle}$ (the uncertainty in the calculated value of $\langle A \rangle$). Therefore, in the plot of $\sigma_B/\sqrt{M_B}$ vs B, a plateau is reached when $B\Delta t$ is much larger than the correlation time, indicating convergence (blue curve in Figure S1b). A constant rising trend instead indicates a high level of correlation (red curve in Figure S1b), and finally a flat trend is synonym of absence of correlation. Notice that while the achievement of convergence of the estimator of $\sigma_{\langle A \rangle}$ depends on the physics of the system through requirement of the total time span $N \times \Delta t$ being much larger than the correlation time, the specific converged value $\sigma_{\langle A \rangle}$ value is statistically dependent on the dimension N of the data

set and decreases as $1/\sqrt{N}$. This observation explains the different plateau values reached in Figure S1b for data sets of different dimensions.

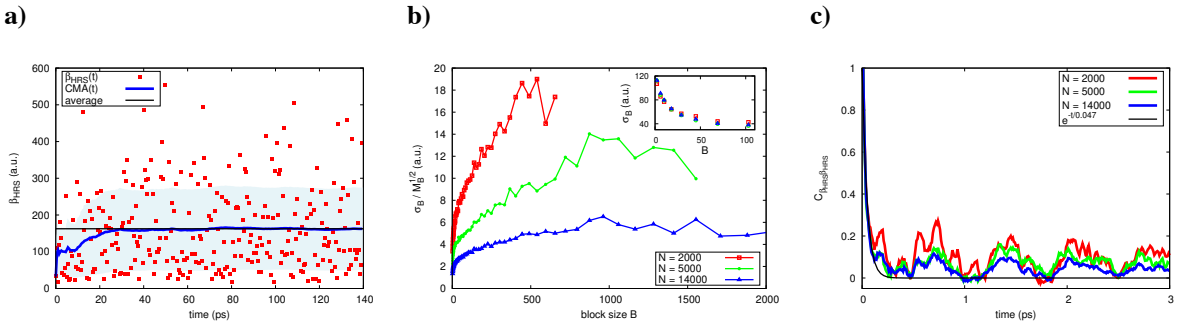

Figure S1: Convergence analyses of azobenzene β_{HRS} obtained from MD trajectories (GAFF model). a) instantaneous values, cumulative average and overall average for a set of $N = 14000$ conformations, sampled every 10 fs. b) normalized $\sigma_B/\sqrt{M_B}$ for β_{HRS}, and in the inset, bare standard deviation of the mean σ_B, calculated for different block sizes B and progressively increasing the dataset size N. c) Autocorrelation functions for different sizes N and exponential fit of the decay at short times.

Convergence and correlation times can be more comprehensively assessed from the decay of the autocorrelation function C_{AA}, whose normalized version is given by the ensemble average:

$$C_{AA}(t) = \frac{\langle A(\tau)\, A(t+\tau)\rangle - \langle A\rangle^2}{\sigma^2}$$

where the main term $\langle A(\tau)\, A(t+\tau)\rangle$ is averaged also over all the available time origins τ. Convergence is achieved when a plateau is reached with $C_{AA}(t) = 0$ (see Figure S1c). The area under the curve is instead the total correlation time, which often is the result of a (multi)exponential decay and can be obtained from a corresponding fit. Alternatively, one can obtain the full frequency power spectrum $S_A(\omega)$ by exploiting the Wiener-Khinchin theorem (see e.g. Ref. 2): $S_A(\omega) = \int_{-\infty}^{\infty} C_{AA}(t)e^{-i\omega t}dt$. Though powerful, the computation of autocorrelation functions requires a good sampling at all the (unknown and system-dependent)

important frequencies, and consequently a more substantial computational effort with respect to the simpler cumulative and block averages.

Table S1. Static and dynamic HRS response of azobenzene (a. u.) calculated at the M06-2X/6-311+G(d) level for different geometries. MD simulations were carried out with NAMD[3] for a single azobenzene molecule in vacuum at 500 K using a Langevin thermostat with a damping factor of 0.2 ps^{-1}. Simulation results are given as of average±standard deviation and, between parentheses, median±interquartile range. "min" stands for equilibrium geometries obtained by minimization with Gaussian16 or NAMD. GAFF is the well-known molecular mechanics force field, while mGAFF is a modified version tailored on azobenzene, in which the equilibrium bond length for the azo bond was adjusted from the default value of 1.2710 Å to the B3LYP/cc-pVTZ value of 1.2484 Å, and the torsional potentials for CNNC and CCNN dihedrals were also refitted against DFT calculations. Notice that with standard GAFF parameters (and B3LYP/cc-pVTZ atomic charges, in this case), the azobenzene equilibrium geometry is erroneously predicted with the NN bond lying on a plane perpendicular to the ones of the phenyl rings.

Structures	DFT min	GAFF min	mGAFF min	GAFF MD, 140 ps	mGAFF MD, 20 ps
β_{HRS}, static	0.01	0.35	0.74	$1.6 \cdot 10^1 \pm 1.1 \cdot 10^1$ $(1.4 \cdot 10^1 \pm 1.6 \cdot 10^1)$	$1.2 \cdot 10^1 \pm 0.70 \cdot 10^1$ $(1.0 \cdot 10^1 \pm 0.84 \cdot 10^1)$
β_{HRS}, dynamic ($\lambda = 1064$ nm)	0.03	0.42	1.70	$0.26 \cdot 10^6 \pm 2.1 \cdot 10^6$ $(4.2 \cdot 10^2 \pm 6.5 \cdot 10^2)$	$0.13 \cdot 10^4 \pm 1.4 \cdot 10^4$ $(3.0 \cdot 10^2 \pm 2.7 \cdot 10^2)$

Modeling the effects of the surrounding environment

Besides explicit one-level treatments, which are restricted to small systems (including the chromophore with a few neighboring molecules) or to simplified methods (sTD-DFT), the surrounding can be described at a lower level of approximation. A very popular choice is the use of Polarizable Continuum Models (PCMs)[4], that associate the solvent to a structureless polarizable medium characterized by, among other parameters, its macroscopic dielectric permittivity, which depends on the frequency of the applied field, while apparent surface charges on the solute-shaped cavity describe the self-consistent reaction field between the solute and the solvent. Alternatively, point charge embeddings (PCEs) treat the surrounding at atomic level and consider its electrostatic/polarization effects,[5] either when it is a solvent or other molecules in more (SAMs) or less (NPs) organized supramolecular structures. Among these, the averaged solvent electrostatic configuration (ASEC) scheme,[6] where the PC values are averages over the different snapshots, present practical advantages for describing the dynamical effects associated with the solvent. Further improvements also include the field-induced effects on the surrounding, adopting polarizable embedding (PE) schemes using either induced dipoles[7] or fluctuating charges.[8] These PE schemes enable to account for both dynamic reaction field and effective local field contributions on the NLO responses, as well as for specific solute-solvent interactions like H-bonds.

Quantum chemical calculations of β and the choice of (time-dependent) DFT

Considering the size of the chromophores (with, if necessary, a few surrounding molecules, either solvent molecules or counterions) as well as the number of snapshots required for an adequate sampling, the range of first principles methods to calculate (electronic) β is in practice restricted to (TD)-DFT and the related quadratic response methods.[9] A key task is therefore to

find reliable approximations to the exchange-correlation (XC) energies, potentials, and kernels, which can be substantiated by comparisons with high-level wavefunction calculations on representative compounds. These reference calculations generally demonstrate that most of the electron correlation effects are included when employing Møller-Plesset second-order perturbation theory, which gives good agreement with coupled cluster (CC) methods including singles and doubles and a perturbative treatment of the triples, CCSD(T).[10] These latter methods are enacted within the finite field approach, providing only comparisons for static quantities. For dynamic responses, as well as the related frequency-dispersion coefficients,[11] reference calculations at the CC2 (second-order CC), CCSD, and CC3 (third-order CC) levels are scarce, usually restricted to much smaller molecules, yet demonstrating the general reliability of CCSD with respect to CC3.[12]

Owing to the intrinsic nonlocal character of electric field effects and to the fact that the β response of push-pull π-conjugated compounds is associated with excitation-induced/field-induced charge transfer, the XC functionals should contain a substantial amount of Hartree-Fock (HF) exchange because it displays the correct $-1/r$ asymptotic behavior. This condition can be (partially) fulfilled using global hybrids, where the amount of HF exchange does not depend on the interelectronic distance, provided this amount is large, like in the M06-2X XC functional (54%). The latter has been shown to well reproduce both experimental data and MP2 reference values for a large set of merocyanines.[13] Alternatively, range-separated hybrids (RSHs) can be employed, where i) the Coulomb operator is split into short- and long-range parts by using a smooth function and ii) the short-range part is associated with local/semilocal exchange and the long-range part with HF exchange. The value of the range-separating parameter, which defines the switch distance between the short- and long-range regions, can be either fixed or optimized to satisfy Koopmans' theorem.[14] Several studies demonstrated that RSHs perform better than local/semilocal functionals but i) the better reliability with respect to

global hybrids is not systematic and, ii) tuning the range-separating parameter does not necessarily improve the accuracy on β, contrary to that of the excitation energies (which is, however, of importance because these latter drive the frequency dispersion of β responses).[13,15,16] Alternatives consist in using a modified version of the multiplicative scheme,[17] where frequency dispersion of the β response is described at the TD-DFT level (with a tuned-RSH TD-DFT) while the MP2 method is used to evaluate the static β responses. Alternatively, the TD-DFT excitation energy of the dominant low-energy dipole-allowed excited state can be employed within a (damped) two-state approximation to describe the frequency dispersion.[18]

A cost-effective alternative to TD-DFT calculations consists in using the simplified TD-DFT scheme (sTD-DFT)[19] which can be applied to systems containing hundreds or thousands of atoms, therefore accounting either for aggregation or explicit surrounding effects. sTD-DFT is based on three approximations (simplified equations for two-electron integrals, truncation of the excited state manifold, and no exchange-correlation kernel) and requires system-specific parameterizations, which can be benchmarked on static and dynamic β responses of representative compounds. A tight-binding implementation of the sTD-DFT method (sTD-DFT-xTB), as well as a version restricted to valence molecular orbitals (sTD-DFT-vTB), have been also developed to further decrease the computational needs.

Like any semi-empirical model, sTD-DFT inherits in principle the accuracy of the reference method used for the parameterization. The reliability of the sTD-DFT-xTB scheme has been recently investigated by its developers for the calculation of the first hyperpolarizabilities of three types of systems: push-pull π-conjugated compounds, fluorescent proteins (eGFP, SHardonnay, DsRed) and a collagen model.[20] For push-pull systems, sTD-DFT was shown to provide dynamic β values very similar to the TD-DFT ones when frequency dispersion effects are small, while further developments are still needed to improve the treatment of resonance

enhancements. In the case of for the fluorescent proteins, sTD-DFT-xTB was shown to outperform standard HF and BHandHLYP calculations with respect to reference MP2/6-31+G(d) calculations, while it reproduced the trends obtained at the ONIOM MP2:HF level for the eGFP chromophore within its first shell of residues. For the collagen model, sTD-DFT-xTB was shown to reproduce the β_{HRS} value from ONIOM LC-BLYP:HF calculations to within less than 10% error.

Obviously, the choice of the right level of approximation is also key for computing third-order NLO contributions, *i.e.* second hyperpolarizabilities. It is for instance of particular relevance for computing EFISHG responses (γ_{EFISHG}, equation 3 of the main text). When the second-order response to γ_{EFISHG} is small, EFISHG becomes governed by its third-order response, $\gamma_{//}(-2\omega;\omega,\omega,0)$. The evaluation of the latter also requires careful description of electron correlation and frequency dispersion effects. However, there are fewer studies on the performance of DFT XC functionals for calculating γ of organic chromophores than on β, usually highlighting the importance of including appropriate amounts of HF exchange. [21,22,23]

Electronic versus vibrational hyperpolarizabilities

Within the Born-Oppenheimer approximation, the effects of electric fields on the electronic and nuclear motions are considered sequentially rather than simultaneously, leading to the decomposition of the whole (hyper)polarizabilities into electronic and vibrational contributions. In their works, by employing perturbation theory, Bishop and Kirtman[24] showed that the total response is divided into i) an electronic contribution involving a zero-point vibrational averaging over the vibrational wavefunction (*e.g.*, $\beta^e + \Delta\beta^{ZPVA}$) and ii) a pure vibrational contribution (β^{pv}).

The ZPVA corrections present therefore the same type of frequency dependence as the electronic term. Few calculations on organic chromophores have shown that $\Delta\beta^{ZPVA}$ amounts to about 10% of the electronic contribution,[25] while for $\Delta\gamma^{ZPVA}$ there are even fewer investigations and they tend to confirm this trend.[26] Since these ZPVA contributions are small and computationally demanding (at first-order of anharmonicity, cubic force constants have to be evaluated, as well as first- and second-order derivatives of the hyperpolarizabilities with respect to the vibrational normal mode coordinates), they are usually not calculated for those conformers being minima on the potential energy surface (QM and QM-MB approaches of Figure 1). By definition, they are not included in the RB-MC calculations. On the other hand, the MD configurations sample, albeit classically, the different vibrational degrees of freedom and therefore the subsequent DFT calculations of the molecular properties account for their zero-point vibrational averaging.

The pure vibrational contributions have different properties than the ZPVA ones: i) their frequency dispersions are small for optical frequencies below the electronic resonances of the chromophores while ii) their amplitudes in comparison to the electronic counterpart depend on the type of NLO process occurring. This is known as the infinite optical frequency[27] or enhanced[28] approximation. So, on the one hand, for all-optical phenomena (like SHG β) those contributions are small and usually neglected in calculations of the NLO responses of stable conformers of chromophores.[29] Indeed, the all-optical pure vibrational contributions are damped by $(\omega_a/\omega)^{2n}$ multiplicative factors (with $n \geq 1$; ω_a and ω are normal mode vibrational frequencies and frequency of the incident light, respectively). On the other hand, for NLO processes involving one or more static electric fields, the pure vibrational contributions can be of the same order of magnitude as their electronic counterparts and cannot be neglected.[26,30] This is thus the case of $\gamma(-2\omega;\omega,\omega,0)$, of which the dominant pure vibrational contribution reads $\frac{1}{4}[\mu\beta]^0_{\omega=0}$ in the infinite optical frequency approximation.[27] For typical push-

pull π-conjugated chromophore, the $\frac{1}{4}[\mu\beta]^0_{\omega=0}$ contribution has been shown to be of the order of 10-20% of the static electronic counterpart. At optical frequencies, owing to the enhancement of $\gamma^e(-2\omega;\omega,\omega,0)$ as a function of ω while $\frac{1}{4}[\mu\beta]^0_{\omega=0}$ can be assumed to be constant, the relative amplitude of the pure vibrational contribution decreases. All in all, for compounds with non-vanishing $\mu_0\beta_{//}(-2\omega;\omega,\omega)$ responses, the $\gamma_{//}(-2\omega;\omega,\omega,0)$ contribution to γ_{EFISHG} is small and its pure vibrational contribution even smaller. On this basis, reliable calculations of the γ_{EFISHG} responses do not need evaluating the pure vibrational counterpart. Nevertheless, there remains an interest to quantify this simplification, in particular when accounting for solvent effects (most of the studies on pure vibrational hyperpolarizabilities of chromophores concern isolated species). At the level of the QM and QM-MB approach, calculating the $\frac{1}{4}[\mu\beta]^0_{\omega=0}$ term is less cost-effective than calculating the ZPVA contribution to γ. It requires evaluating the first-order derivatives of the dipole moment (related to IR intensities) and of the first hyperpolarizabilities (related to hyper-Raman intensities) with respect to the vibrational normal mode coordinates.

Table S2: Recent studies employing sequential MD+QM calculations for evaluating the impact of structural fluctuations on the NLO responses of various molecules and aggregates.

System	MD	QM	Environment	Property	Reference
Tetranitrotetra-propoxycalix[4]arene	CHARMm	projection on reference structures of known INDO/CIS hyperpolarizability	none	HRS	Kenis *J. Am. Chem. Soc.* **1998**, *120*, 7875
Pyridine-pyrimidine and hydrazone-pyrimidine foldamers	MMFF94	TDHF	none	HRS, EFISHG	Méreau, *J. Phys. Chem. A* **2009**, *113*, 6552
Nitrobenzene/benzene solutions	rigid-body Monte Carlo	TDHF	PCM, PCE, explicit	HRS, EFISHG	Hidalgo Cardenuto, *J. Chem. Phys.* **2014**, *141*, 234104
Indolino-oxazolindine/diarylethene biphotochromic switch	rigid-body Monte Carlo	TDHF	PCM, PCE	HRS	Quertinmont, *J. Phys. Chem. A*, **2015**, *119*, 5496
Laurdan and C-Laurdan in DOPC lipid bilayers	GAFF	TD-DFT (CAM-B3LYP)	PCM	TPA, EFISHG	Osella, *J. Chem. Theory Comput.* **2016**, *12*, 6169
Disubstituted benzenes	Amber 99ffSB-ILDN	TD-DFT (CAM-B3LYP)	PCE, PE	HRS	Giovannini, *Theor. Chem. Acc.* **2018**, *137*, 74
Indolino-oxazolidine photoswitches + counterion for POF	Amber (reparameterized)	TDDFT (M06-2X)	PCM	HRS, EFISHG	Pielak, *J. Phys. Chem. C.* **2018**, *122*, 26160
SAMs based on indolino-oxazolidine photoswitches	Amber (reparameterized)	TD-DFT (M06-2X)	none	SHG	Tonnelé, *Phys. Chem. Chem. Phys.* **2018**, 20, 21590
SAMs based on azobenzene photoswitches	Amber (reparameterized)	TD-DFT (M06-2X, CAM-B3LYP)	none, PCE	SHG	Tonnelé, *Chem. Mater.* **2019**, 31, 6759
Tryptophane-rich peptides and gramicidin A	meta-dynamics/ GFN2-xTB and conformer selection using DFT	sTD-DFT-xTB	GBSA continuum	HRS	Seibert, *J. Phys. Chem. B* **2020**, 124, 2568
Stilbazolium ion pairs	OPLS-AA (reparameterized)	TDDFT (M06-2X)	PCM	HRS, EFISHG	Ramos, *J. Chem. Inf. Model.* **2020**, 60, 4817
p-Nitroaniline	GAFF	MP2	PCE, PE	HRS, EFISHG	Hrivnak, *J. Phys. Chem. A* **2020**, 124, 10195
Dimeric aggregates of stilbazolium ion pairs	OPLS-AA (reparameterized)	TDDFT (M06-2X)	IEF-PCM	HRS, EFISHG	Ramos, *J. Phys. Chem. B* **2021**, 125, 3386
Di-8-ANEPPS in phosphatidylcholine lipid bilayers	GAFF (reparameterized)	TDDFT (M06-2X)	PCE + PCM	SHG	Bouquiaux, *J. Phys. Chem. B* **2021**, 125, 10195
Organic nanoparticles based on push-pull chromophores	Amber (reparameterized)	sTDDFT	explicit	HRS	Lescos, *Phys. Chem. Chem. Phys.* **2021**, 23, 23643

References

[1] Grossfield, A.; Zuckerman, D. M. Chapter 2: Quantifying Uncertainty and Sampling Quality in Biomolecular Simulations, *Annual Reports in Computational Chemistry*, **2009**, *5*, 23-48.

[2] Koyama, A.; Nicholson, D. A.; Andreev, M.; Rutledge, G. C.; Fukao, K.; Yamamoto, T. Spectroscopic analysis in molecular simulations with discretized Wiener-Khinchin theorem for Fourier-Laplace transformation, *Phys. Rev. E* **2020**, *102*, 063302.

[3] Phillips, J. C; et al. Scalable molecular dynamics on CPU and GPU architectures with NAMD, J. Chem. Phys. **2020**, *153*, 044130.

[4] Tomasi, J.; Mennucci, B.; Cammi, R. Quantum Mechanical Continuum Solvation Models, *Chem. Rev.* **2005**, *105*, 2999-3094.

[5] Quertinmont, J.; Champagne, B.; Castet, F. Hidalgo Cardenuto Explicit versus Implicit Solvation Effects on the First Hyperpolarizability of an Organic Biphotochrome *J. Phys. Chem. A*, **2015**, *119*, 5496-5503.

[6] Coutinho, K.; Georg, H.C.; Fonseca, T.L.; Ludwig, V.; Canuto, S. An efficient Statistically Converged Average Configuration for Solvent Effects, *Chem. Phys. Lett.*, **2007**, *437*, 148-152.

[7] List, N.H.; Jensen, H.J.A. Kongsted, J.; Local Electric Fields and Molecular Properties in Heterogeneous Environments Through Polarizable Embedding, *Phys. Chem. Chem. Phys.* **2016**, *18*, 10070–10080.

[8] Giovannini, T.; Ambrosetti, M.; Cappelli, C. A Polarizable Embedding Approach to Second Harmonic Generation (SHG) of Molecular Systems in Aqueous Solutions, *Theor. Chem. Acc.* **2018**, *137*, 74.

[9] Helgaker, T.; Coriani, S.; Jørgensen, P.; Kristensen, K.; Olsen, J.; Ruud, K. Recent Advances in Wave Function-Based Methods of Molecular-Property Calculations *Chem. Rev.* **2012**, *112*, 543-631.

[10] de Wergifosse, M.; Champagne, B. Electron Correlation Effects on the First Hyperpolarizability of Push-Pull π-Conjugated Systems, *J. Chem. Phys.* **2011**, *134*, 074113.

[11] Hättig, C.; Jørgensen, P. Dispersion Coefficients for First Hyperpolarizabilities from Coupled Cluster Quadratic Response Theory, *Theor. Chem. Acc.* **1998**, *100*, 230-240.

[12] Salek, P.; Helgaker, T.; Vahtras, O.; Ågren, H.; Jonsson, D.; Gauss, J. A Comparison of Density-Functional-Theory and Coupled-Cluster Frequency-Dependent Polarizabilities and Hyperpolarizabilities, *Mol. Phys.* **2005**, *103*, 439-450.

[13] Lescos, L.; Sitkiewicz, S. P.; Beaujean, P.; Blanchard-Desce, M.; Champagne, B.; Matito, E.; Castet, F. Performance of DFT Functionals for Calculating the Second-Order Nonlinear Optical Properties of Dipolar Merocyanines. *Phys. Chem. Chem. Phys.* **2020**, *22*, 16579-16594.

[14] Kronik, L.; Stein, T.; Refaely-Abramson, S.; Baer, R. Excitation Gaps of Finite-Sized Systems from Optimally Tuned Range-Separated Hybrid Functionals, *J. Chem. Theory Comput.* **2012**, *8*, 1515-1531

[15] Sun, H.; Autschbach, J. Influence of the Delocalization Error and Applicability of Optimal Functional Tuning in Density Functional Calculations of Nonlinear Optical Properties of Organic Donor-Acceptor Chromophores. *ChemPhysChem*. **2013**, *14*, 2450–2461.

[16] Garrett, K.; Sosa Vazquez, X.A.; Egri, S. B.; Wilmer, J.; Johnson, L.E.; Robinson, B.H.; Isborn, C.M., Optimum Exchange for Calculation of Excitation Energies and Hyperpolarizabilities of Organic Electro-Optic Chromophores, *J. Chem. Theory Comput.* **2014**, *10*, 3821-3831.

[17] Sekino, H.; Bartlett, R.J. Hyperpolarizabilities of Molecules with Frequency Dependence and Electron Correlation, *J. Chem. Phys.* **1991**, *94*, 3665-3669.

[18] de Wergifosse, M.; Liégeois, V.; Champagne, B. Evaluation of the Molecular Static and Dynamic First Hyperpolarizabilities, *Int. J. Quantum Chem.* **2014**, *114*, 900-910.

[19] de Wergifosse, M.; Grimme, S. Perspective on Simplified Quantum Chemistry Methods for Excited States and Response Properties, *J. Phys. Chem. A*, **2021**, *125*, 3841–3851.

[20] de Wergifosse M.; Grimme, S. Nonlinear-response properties in a simplified time-dependent density functional theory (sTD-DFT) framework: Evaluation of the first hyperpolarizability, *J. Chem. Phys.*, **2018**, *149*, 024108.

[21] Bulat, F.E.; Toro-Labbé, A.; Champagne, B.; Kirtman, B.; Yang, W. Density-Functional Theory (Hyper)Polarizabilities of Push-Pull π-Conjugated Systems: Treatment of Exact Exchange and Role of Correlation, *J. Chem. Phys.* **2005**, *123*, 014319.

[22] Baranowska-Laczkowska, Bartkowiak, W.; Gora, R.W., Pawlowski, F.; Zalesny, R. On the Performance of Long-Range-Corrected Density Functional Theory and Reduced-Size Polarized LPol-n Basis Sets in Computations of Electric Dipole (Hyper)Polarizabilities of π-Conjugated Molecules, *J. Comput. Chem.* **2013**, *34*, 819-826.

[23] Besalu-Sala, P.; Sitkiewicz, S.; Salvador, P.; Matito, E.; Luis, J.M. A New Tuned Range-Separated Density Functional for the Accurate Calculation of Second Hyperpolarizabilities, *Phys. Chem. Chem. Phys.* **2020**, *22*, 11871-11880.

[24] Bishop, D.M.; Kirtman, B. A Perturbation Method for Calculating Vibrational Dynamic Dipole Polarizabilities and Hyperpolarizabilities, *J. Chem. Phys.* **1991**, *95*, 2646-2658.

[25] Quinet, O.; Kirtman, B.; Champagne, B. ZPVA Correction to the Dynamic First Hyperpolarizability of Para-Nitroaniline, *J. Molec. Struct. (THEOCHEM)* **2003**, *633*, 199-207.

[26] Torrent-Sucarrat, M.; Sola, M.; Duran, M.; Luis, J.M.; Kirtman, B. Basis Set and Electron Correlation Effects on Initial Convergence for Vibrational Nonlinear Optical Properties of Conjugated Organic Molecules, *J. Chem. Phys.* **2004**, *120*, 6346-6355.

[27] Bishop, D.M.; Hasan, M.; Kirtman, B., A Simple Method for Determining Approximate Static and Dynamic Vibrational Hyperpolarizabilities, *J. Chem. Phys.* **1995**, *103*, 4157-4160.

[28] Elliott, D.S.; Ward, J.F. Vibrational Mode Contributions to Molecular Third Order Polarizabilities, *Mol. Phys.* **1984**, *51*, 45-63.

[29] Gao, B.; Ringholm, M.; Bast, R.; Ruud, K.; Thorvaldsen, A.J.; Jaszunski, M. Analytic Density Functional Theory Calculations of Pure Vibrational Hyperpolarizabilities: The First Dipole Hyperpolarizability of Retinal and Related Molecules, *J. Phys. Chem. A* **2014**, *118*, 748-756.

[30] Champagne, B.; Kirtman, B. Vibrational versus Electronic First Hyperpolarizabilities of π-conjugated Organic Molecules: An Ab Initio Hartree-Fock Investigation upon the Effects of the Nature of the Linker, *Chem. Phys.* **1999**, *245*, 213-226.